IOP PUBLISHING NANOTECHNOLOGY
Nanotechnology **18** (2007) 285602 (9pp) doi:10.1088/0957-4484/18/28/285602

Magnetic iron oxide/clay composites: effect of the layer silicate support on the microstructure and phase formation of magnetic nanoparticles

Tamás Szabó[1], Aristides Bakandritsos[2], Vassilios Tzitzios[2], Szilvia Papp[3], László Kőrösi[3], Gábor Galbács[4], Kuanyshbek Musabekov[5], Didara Bolatova[5], Dimitris Petridis[2] and Imre Dékány[1,3]

[1] Department of Colloid Chemistry, University of Szeged, Aradi vértanúk tere 1, H-6720 Szeged, Hungary
[2] Institute of Materials Science, National Center for Scientific Research (NCSR) 'Demokritos', Agia Paraskevi, 15310, Athens, Greece
[3] Nanostructured Materials Research Group of the Hungarian Academy of Sciences, University of Szeged, Aradi vértanúk tere 1, H-6720 Szeged, Hungary
[4] Department of Inorganic and Analytical Chemistry, University of Szeged, Dóm tér 7, H-6720, Hungary
[5] Department of Chemistry, Kazakh National State University named Al-Faraby, Karasay Batyr 95, Almaty, 480012, The Republic of Kazakhstan

E-mail: sztamas@chem.u-szeged.hu and i.dekany@chem.u-szeged.hu

Received 15 March 2007, in final form 26 April 2007
Published 15 June 2007
Online at stacks.iop.org/Nano/18/285602

Abstract
Magnetic iron oxide nanoparticles were synthesized on two different clay supports: natural montmorillonite and synthetic laponite. The nanocomposites obtained, characterized by inductively coupled plasma atomic emission spectroscopy (ICP-AES), x-ray diffraction (XRD), transmission electron microscopy (TEM), N_2 adsorption, small-angle x-ray scattering (SAXS), vibrating sample magnetometry and Mössbauer spectroscopy, were found to exhibit highly different physicochemical properties despite their similar iron content. The observed size effect of the layered silicate support, resulting in the high abundance of very small particles (diameter of 1–5 nm) on laponite, was explained in terms of the difference between the surface charge densities and the lamellar dimensions of the clay substrates. Moreover, it was revealed that the nature of the layered support greatly affected the nanostructure (fractal dimensions, surface area, porosity) of the formed hybrid solids as well as the phase formation of iron oxide crystals. The high surface area laponite composites, due to the dominance of very small iron oxide particles, exhibited more pronounced superparamagnetic behaviour as compared to the montmorillonite samples prepared under identical conditions. The observed higher saturation magnetization of the laponite composites, attributed to their lower content in the antiferromagnetic hematite and to the onset of superferromagnetism in the aggregated particles, shows their excellent utility for adsorption/magnetic separation.

1. Introduction

Bare and coated magnetic nanocrystals, either free-standing or immobilized, are exploited in an increasing number of chemical, biochemical or environmental applications. Magnetite is an iron catalyst with a central role in the industrial Haber–Bosch process for the production of ammonia [1, 2]. Magnetic nanoparticles and their composites are extremely suitable in water treatment for the coagulation of sewage [3] or for the complete elimination of contaminants from drinking water sources such as heavy metals [4] or dissolved organic matter such as humic and fulvic acids [5, 6] without posing any danger to the human organism. Besides these conventionally considered fields, magnetic materials became highlighted in nanoscience, medicine, and biotechnology, serving as high-density recording media [7], novel recoverable enzyme or drug carriers [8–10] or tools for the separation and purification of biomolecules and cells in bioprocesses [11, 12].

The marked utility of such subcolloid systems in most of the above applications stems directly from their nanometric size. First, their small diameter results in a much higher specific surface area as compared to coarse particles, which favours their use in catalytic processes. Second, lowering the dimensions of the crystal results in a concomitant decrease in the energy associated with the magnetic anisotropy until the energy of random thermal motion overcomes any preferential orientation of the moment in the particle [7]. Consequently, such ultrafine crystals will exhibit superparamagnetism, that is, they are attracted by an external magnetic field but retain no magnetism after the field ceases. Therefore, superparamagnetic particles can be manipulated and thus separated from the medium using a permanent magnet or an electromagnet. Although the application of an external magnetic field induces aggregation of the particles (resulting in the phenomenon called magnetic ageing) [13], they do not settle down after the removal of the applied field [8].

An important factor to take into account for magnetic separation is the wear between moving surfaces [14]. To slow down the sedimentation and to obtain a soft sediment, the application of antisettling agents is desirable [15]. Smectite-type clay minerals having highly anisometric lamellae can be readily used for this aim and, moreover, their cation-exchange properties make them outstandingly suitable starting materials for the preparation of metal oxide nanocomposites [16–20]. Magnetic iron oxide/montmorillonite hybrid materials have been described in the literature, including both magnetite [14, 21] and maghemite [4, 22, 23]. Nevertheless, these works concern natural clays and, to our knowledge, no work has been performed on synthetic layer silicates which have gained increasing interest in numerous fields of application.

The objective of this work is to extend the field of magnetically modified smectites by introducing laponite, a synthetic product chemically analogous to hectorite [24] but with very small aspect ratio, acting as a support for iron oxide nanoparticles. The structure and characteristics of the laponite composite will be systematically compared to those of a montmorillonite composite prepared under identical conditions.

2. Experimental details

2.1. Synthesis of iron oxide/clay composites

The preparation of magnetically modified layered silicates relies on the method developed by Bourlinos *et al* [22]. 1 g of Na-montmorillonite (EXM838 from Süd-Chemie AG, Germany), abbreviated hereafter as Mont, was dispersed in 50 ml of distilled water, and 100 ml of 0.02 M $FeCl_3 \cdot 6H_2O$ (pH adjusted to 2.5 by NaOH) was added dropwise under stirring. After stirring for 20 min the suspension was centrifuged and washed three times with water. The intercalation procedure was repeated twice more in the same manner, then the wet sediment was spread over a glass plate and dried in air. The film was exposed to excess glacial acetic acid vapours for 2 h at 80 °C, crushed into powder and calcined in air at 400 °C for 2 h to get the magnetic clay composite (denoted as Fe-Mont1). Two further composites with higher expected iron loading were also prepared by adding 150 or 200 ml of the $FeCl_3$ solution to give samples of Fe-Mont2 and Fe-Mont3, respectively.

Magnetic derivatives of Na-laponite (Solvay, Germany) were obtained by the same procedure using lyophilized and dialysed clay specimens (Lap). Notations for the composites are Fe-Lap1 (100 ml of added $FeCl_3$ solution), Fe-Lap2 (150 ml) and Fe-Lap3 (200 ml).

2.2. Characterization techniques

The iron content of the samples was determined by inductively coupled plasma atomic emission spectroscopy, using a sequential all-argon Jobin-Yvon 24 type spectrometer equipped with a sample introduction system consisting of a Gilson Minipuls III peristaltic pump, a Teflon V-groove nebulizer and a Scott type double pass spray chamber. For each sample, three parallel determinations were performed at the 238.2 nm emission wavelength.

XRD measurements were performed on a Philips PW 1830 diffractometer operating with a Cu anode (40 kV, 30 mA). Cu Kβ radiation was absorbed by a nickel filter.

TEM images were taken on a Philips CM-10 electron microscope operating at a 100 kV accelerating voltage. The composites were dispersed in ultrapure water and aliquots from the liquid were dropped on Formvar-coated copper grids. The particle diameters were determined by the UTHSCSA Image Tool program.

N_2 adsorption isotherms on samples kept previously in vacuum for 2 h were determined at 77 K in a Micromeritics Gemini 2375 automated sorptometer.

For small-angle x-ray scattering (SAXS) investigations, Cu Kα x-radiation was generated in a PW 1830 source. The primary beam of 20 mm width and 80 μm thickness was directed through a Ni filter into an evacuated KCEC/3 type compact Kratky camera where it scattered on the powdered composites fixed in a 0.5 mm thick copper sample holder perpendicular to the beam. The intensity of the scattered radiation was measured by a MBraun PSD 50M type position-sensitive x-ray detector having 1024 channels in the 2Θ range 0.05°–7°. The absolute values of scattering intensities of the samples, determined by the moving-slit method, were normalized and corrected with that of the background.

Table 1. Total iron contents, contents and particle sizes of iron(III) oxide, densities and saturation magnetizations of pristine and derived clays.

Sample	Fe content (wt%)	Fe_2O_3 content (wt%)	Particle size (nm)	Density (g cm^{-3})	M_S (emu g^{-1})
Mont	0.38 ± 0.01	—	—	2.47	—
Fe-Mont1	19.8 ± 0.8	27.8 ± 1.1	17 ± 9	3.20	—
Fe-Mont2	22.8 ± 0.8	32.1 ± 1.1	16 ± 6	3.20	8.56
Fe-Mont3	22.4 ± 0.8	31.5 ± 1.1	15 ± 8	3.20	—
Lap	—	—	—	2.16	—
Fe-Lap1	17.2 ± 0.4	24.6 ± 0.6	2.3 ± 0.9	2.92	—
Fe-Lap2	22.4 ± 0.3	32.1 ± 0.4	2.9 ± 0.9	2.92	12.8
Fe-Lap3	21.9 ± 0.2	31.2 ± 0.3	1.8 ± 0.8	2.92	—

The density of the samples used for SAXS calculations was measured by a helium pycnometer (Micromeritics 1305).

Mössbauer spectra were recorded with a constant acceleration spectrometer with a 50 mCi ^{57}Co(Rh) source moving at room temperature, while the sample was placed in a variable temperature cryostat. Isomer shift values are reported with respect to α-Fe.

Magnetic measurements were carried out at room temperature with a vibrating sample magnetometer (VSM).

3. Results and discussion

3.1. Iron content

The bright reddish-brown colour of each sample, together with their marked macroscopically magnetic behaviour (as probed by a permanent magnet), suggests the abundance of an iron oxide phase in the clay composites. Therefore, iron must be present in the composite in the form of iron(III) oxides, very likely as γ-Fe_2O_3 and α-Fe_2O_3 (hydroxides, oxyhydoxides and magnetite are not stable at the calcination temperature of 400 °C). The total iron contents and the corresponding Fe_2O_3 contents of the samples (table 1) are very high and show no significant differences, which indicates some important points. The iron species adsorbed cannot be a simple aquacomplex as the amount of iron adsorbed (about 3.5 mmol Fe/1 g of clay) would refer to a hypothetic cation-exchange capacity (CEC; about 11.5 mequ g^{-1}) which is more than an order of magnitude higher than that of the smectites used (CEC_{Mont} = 0.85 mequ g^{-1}, CEC_{Lap} = 0.45 mequ g^{-1}). We must point out that the addition of the clay suspension shifts the pH of the iron chloride solution to somewhat higher values (around 3–3.5), at which the Fe(III) begins to hydrolyse. The formed oligo- or polynuclear iron complexes, depending on their charge, can be either immobilized via an ion-exchange mechanism or simply deposited on the silicate surface, and in this way they smear the differences of the CEC values and surface charge densities between the layer silicate supports. Finally, Fe-Mont2, Fe-Mont3, Fe-Lap2 and Fe-Lap3 exhibit the same iron contents, meaning that full loading at the given conditions has been established.

3.2. XRD analysis

Figure 1 shows the XRD patterns of the bare supports (curve A and C) and those of the nanocomposites (curve B and D). The latter, apart from the clay reflections, present some additional peaks that obviously originate from iron oxides.

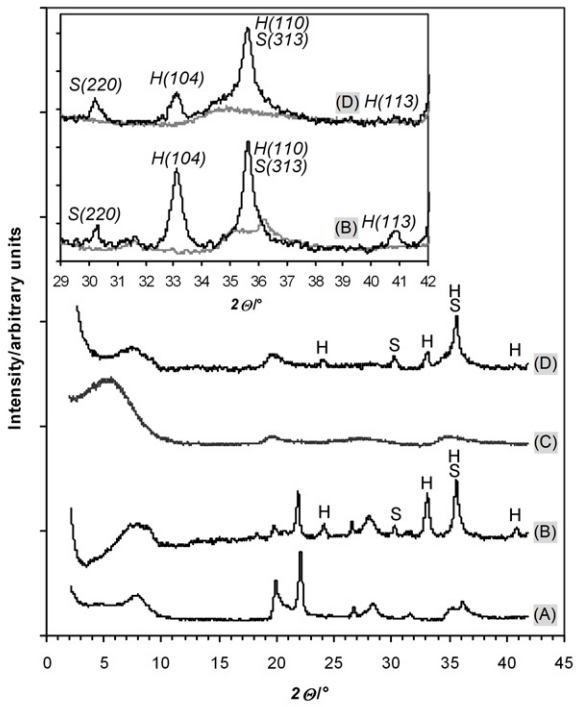

Figure 1. XRD patterns of (A) Mont, (B) Fe-Mont2, (C) Lap and (D) Fe-Lap2. Symbols represent the reflections of the iron oxide phases (S: spinel structure; H: hematite). The inset focuses on the iron oxide reflections including the respective Miller indices.

Comparison of the observed peak positions with the JCPDS database revealed the presence of rhombohedral hematite (card 33-0664) with reflections at $2\Theta = 33.18°$, 35.68° and 40.98°. Besides, the reflections at $2\Theta = 30.24°$ and 35.68°, characteristic for the spinel-type structure (card 39-1346), indicated the formation of either Fe_3O_4 or γ-Fe_2O_3. The $2\Theta = 29°$–42° region involving these iron oxide reflections is enlarged in the inset of figure 1; the diffraction lines at higher angles are not evaluated due to their low intensity or their overlapping with certain reflections of the copper sample holder.

The absolute intensities of the iron oxide reflections (after correction for the background scattering) and the relative intensities (after taking the most intense reflection to 100%) are seen in table 2. The latter are compared with the standard JCPDS diffraction pattern. As the (110) line of hematite appears exactly at the same position (35.68°) as that of the (313) line of the spinel phase, the intensity of this composite

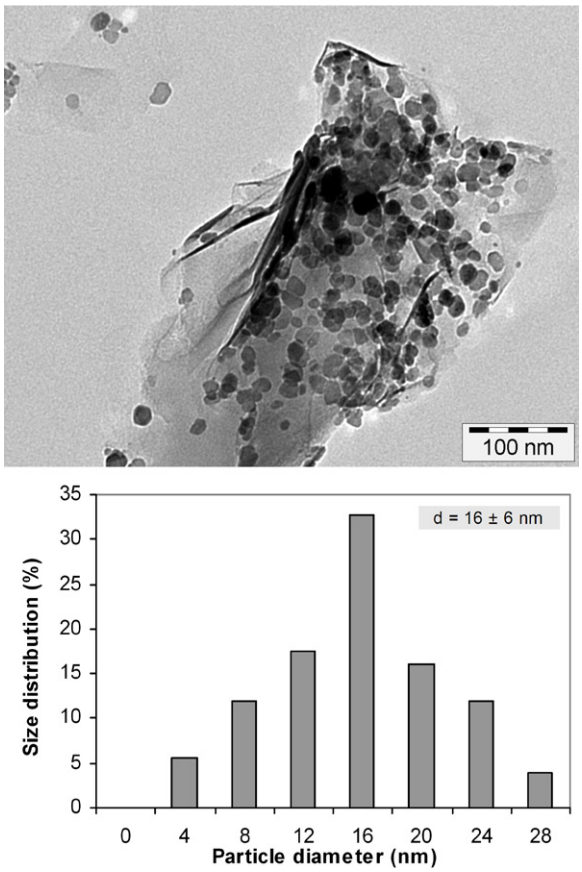

Figure 2. TEM micrograph and particle size distribution (% in number of particles) of Fe-Mont2 composite.

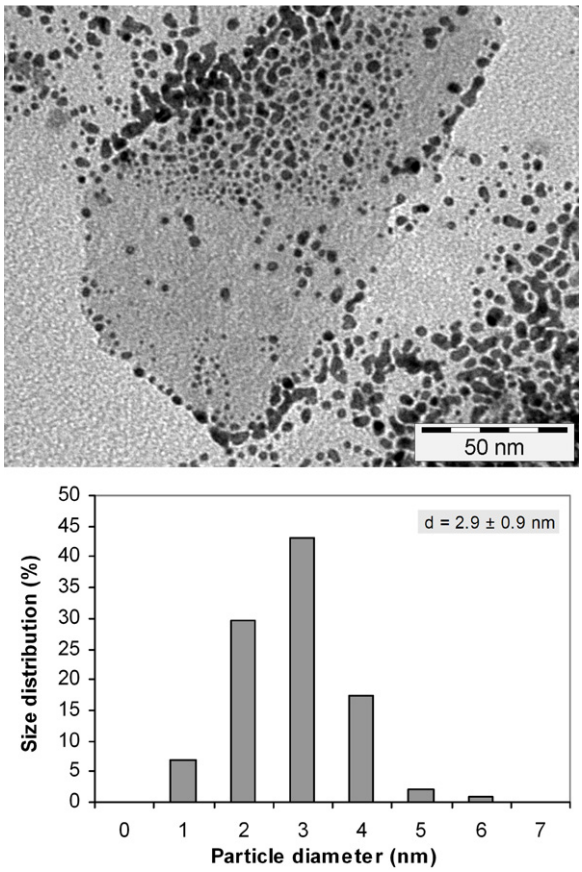

Figure 3. TEM micrograph and particle size distribution (% in number of particles) of Fe-Lap2 composite.

Table 2. XRD parameters of the iron oxides in the composites: Fe_2O_3 phase (S: spinel-type structure, H: hematite), diffraction angles, repeat distances and diffracted x-ray intensities in total counts and %, respectively.

Phase/index	2Θ (deg)	d_{hkl} (nm)	$I_{Fe-Mont2}$ (cps/%)	$I_{Fe-Lap2}$ (cps/%)	I_{JCPDS} (%)
S/220	30.24	0.296	85/33	115/32	30
H/104	33.18	0.270	415/100	170/100	100
S/313	35.68	0.252	260/100	365/100	100
H/110	35.68	0.252	210/50	85/50	50
H/113	40.98	0.220	90/21	30/18	30

peak needs to be separated into two components with respect to the distinct iron oxide phases. For this we assume that hematite crystallites contribute to the total intensity (470 cps for Fe-Mont2 and 450 cps for Fe-Lap2) by 210 and 85 cps, respectively (and the remaining intensity is due to the other phase). This is because, according to the standard hematite pattern, these values are equal to 50% of the intensities of the (104) hematite reflections in Fe-Mont2 and Fe-Lap2. It is apparent that the relative intensities of the reflections agree very well with the standard values for both phases and in both composites. This means that the texture of the samples, that is, the distribution of the crystallographic orientations of the nanocrystals, is identical both in the composites and in the standard JCPDS samples. Consequently, the diffractogram of the composites containing biphase iron oxide can be reliably regarded as a superimposed pattern of the individual phases. The intensity ratios of the most intense spinel (313) and hematite (104) related reflections are 0.62 for Fe-Mont2 and 2.15 for Fe-Lap2. These values do not give direct and quantitative information on the phase ratios. Nevertheless, they do provide evidence that the relative amount of the spinel-type phase is higher (thus the amount of hematite is lower) on laponite than on the other support.

3.3. Electron microscopy

Representative TEM images of the Fe-Mont2 and Fe-Lap2 samples are displayed in figures 2 and 3, respectively. There are spectacular differences in the microstructure of the composites: the nanoparticles formed on montmorillonite are much larger, their surface coverage is higher, and they are dispersed quite homogeneously over the lamellae. On the other hand, the iron oxide dots are very small and are heterogeneously distributed over the laponite support, showing significant and uniform coverage on certain regions of the silicate sheets and near its edges, which is not extended to the whole surface. Moreover, the abundance of freestanding nanoparticles was much more pronounced in this case (see the area near the scale bar in figure 3), indicating that the nanocrystals were removed from the substrate, possibly during the sonication step of the sample preparation for TEM. It should be noted that no traces of unsupported iron oxide

Table 3. SAXS parameters and specific surface areas of the clays and their magnetic derivatives.

Sample	Mont	Fe-Mont1	Fe-Mont2	Fe-Mont3	Lap	Fe-Lap1	Fe-Lap2	Fe-Lap3
D_m	—	2.64	2.65	2.68	—	2.50	2.61	2.75
D_S	2.50	2.97	3.00	2.98	2.98	2.89	3.00	2.97
l_s (nm)	15.3	11.1	10.3	10.2	3.7	3.5	4.2	4.8
l_C (nm)	20.6	14.6	13.9	13.6	3.7	4.7	5.1	6.1
a^S_{SAXS} (m^2 cm^{-3})	262	358	387	390	994	1159	1019	861
a^S_{SAXS} (m^2 g^{-1})	106	112	121	122	460	397	349	295
a^S_{BET} (m^2 g^{-1})	27	66	77	77	307	288	217	185

particles were observed in the several micrographs recorded from the montmorillonite derivatives, suggesting a more efficient particle stabilization on this clay.

The size distribution histograms of Fe-Mont and Fe-Lap composites in figures 2 and 3 were determined by measuring the diameter of 100–150 randomly chosen particles. Due to the total number of counts the diameter axis was scaled by seven or six intervals [25]. Only the spherical crystallites were taken into account, omitting the partially coalesced aggregates with other morphologies for which the particle dimensions can hardly be defined. The particles average 16 nm on montmorillonite, while those immobilized on laponite are five times smaller, ranging from 2 to 3 nm. The significant difference in the diameters clearly shows the size effect of the clay support. We attribute this phenomenon to the difference in the cation-exchange capacities (CECs) of the silicates. Although the adsorbed amounts of iron species are independent of the CEC, the different surface charge densities can play a role in the particle evolution, affecting the nucleation, growth and migration processes. Due to the high density of ion-exchange sites on montmorillonite, the highly charged oligonuclear iron complexes (via electrostatic interactions) are much more strongly bound to the surface than the less charged or neutral species deposited. Therefore, the latter will migrate easily to those localized at the exchange positions, favouring particle growth to nucleation. On the other hand, nucleation obviously dominates over growth in the case of laponite, resulting in the formation of ultrafine particles of 2–3 nm diameter. Owing to the low CEC of laponite, the electrostatically bound iron species located at the few exchange positions are farther from each other. As a consequence, the average migration distance of the rest of the iron complexes to these strongly fixed nucleation centres is also higher on this clay. Therefore, upon the prolonged migration process part of these complexes induce extensive secondary nucleation. Also, the much smaller laponite particles exhibit a higher density of $M–O^{(-)}$ (M = Si, Mg) reactive edge sites than the larger montmorillonite particles (M = Si, Al, Mg, Fe), which readily constitute additional nucleation centres.

Finally, it should be noted that the higher abundance of aggregates and partially coalesced, irregularly shaped clusters of nanoparticles in the laponite composites is in direct correlation with the smaller primary particle dimensions. It is well known that nanocrystals are thermodynamically unstable systems due to their high surface free energy, which is inversely proportional to their radius or diameter. Consequently, the driving force for agglomeration is much higher for the ultrasmall particles grown over laponite.

3.4. SAXS investigations

Small-angle x-ray scattering (SAXS) is a powerful technique for the characterization of colloid systems, especially nanocomposite materials. Any changes in the inhomogeneities characterizing the structure of the disperse system, such as aggregation, surface modification, development of porosity or surface area, directly influences the angular dependence of the scattering vector. The scattering curves are plotted in the lg I versus lg h representation in figure 4, while the most important structural parameters (calculated by procedures described earlier [26–28]), along with the specific surface areas determined by SAXS and N_2 adsorption, can be found in table 3. It is apparent from the difference in the scattering curves, especially in the Porod range ($-1.2 < \lg h < 0.1$) providing most of the useful information on the samples, that the surface modification of clays altered the nanostructure of the solid. The surface fractal dimensions (D_S) of montmorillonite composites, characteristic for the roughness of the surface in the subcolloid range, are higher than that of the pristine clay. This suggests that these derivatives have more crumpled, rougher surfaces due to the presence of nanoparticles. This is not the case for laponite, as it inherently possesses one of the highest fractalities possible. The same deviation applies for the mass fractal dimensions (D_m) derived from the 0.06–0.26 nm^{-1} scattering vector range. D_m values can range between 1 and 3, the former value referring to compact, nonporous structures, and the latter one corresponding to systems of great porosity. All of the composites were found to have highly porous structures (D_m = 2.5–2.75) and the porosity even slightly increased upon iron oxide loading (the mass fractals of the bare clays could not be determined due to the ill-defined slope of their scattering curve).

The correlation lengths (l_c), that is the statistical average distances of inhomogeneities characteristic for the composite/air (solid/gas) disperse system, refer to the nanostructure of the porous material. Again, there is a marked difference between the different substances; moreover, the l_s values (referring to the submicroscopic discontinuities of the solid phase itself) follow the same trend as those of l_c. According to the pure clays, the smaller l_s values for laponite must be primarily due to the smaller lateral dimension of the lamellae. However, a slight contribution can be caused by the fact that the lamellar packages present in the solid are composed of fewer individual sheets, as is apparent from the broader (001) XRD reflections of the laponite (figure 1). The l_c and l_s values for the montmorillonite composites are smaller than that of the pure support, while those of the laponite

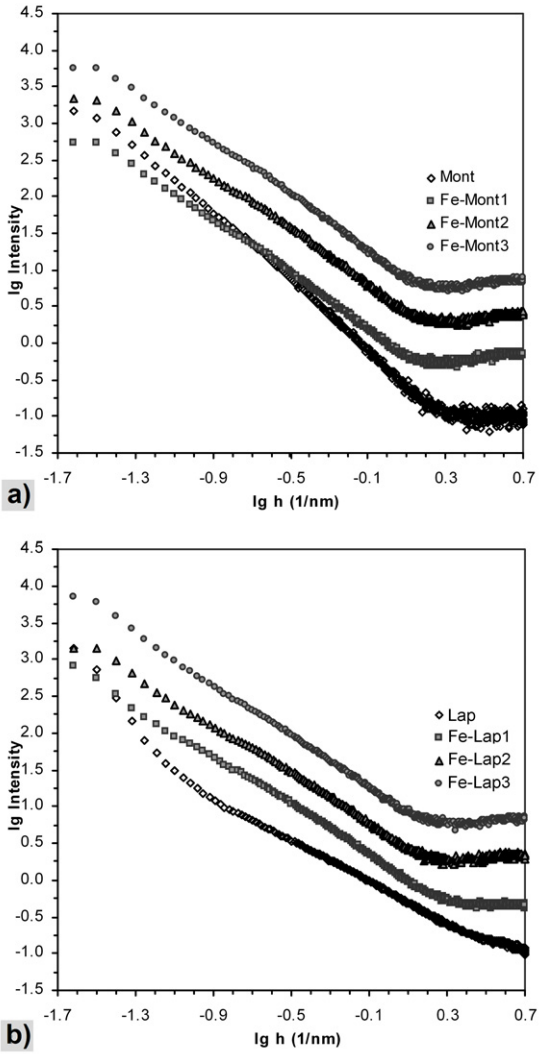

Figure 4. SAXS profiles of pristine and magnetically modified montmorillonite (a) and laponite (b). Curves of Fe-Mont2/Fe-Lap2 and Fe-Mont3/Fe-Lap3 are offset by 0.5 and 1 lg I units, respectively.

composites are nearly identical with the parent silicate. This implies that the montmorillonite sheets are less well stacked in the final product (even though the iron oxide dots migrate to the external surfaces from the intergallery space), while no further dispersion is possible for laponite, whose composites consist of smaller particles matrixed by highly exfoliated clay lamellae.

N_2 adsorption isotherms (not shown) supported the porous nature of the samples and that the specific surface area of laponite and its composites are significantly higher than those derived from montmorillonite. Nevertheless, while the surface area of montmorillonite increased upon iron oxide loading, the opposite trend was detected for laponite. A seemingly obvious explanation (i.e. the iron oxides open up the interlamellar space) fails because in this case the same trend would be expected for laponite specimens and it was already established that the nanoparticles are situated at the external surfaces. The specific surface areas determined by SAXS followed the same change as $a_{\mathrm{BET}}^{\mathrm{S}}$ values, although they were much higher. Since SAXS measures the total surface of the homogeneous scattering centres, it can detect the pores fully closed or inaccessible for the nitrogen molecules at 77 K. Therefore, it can be ruled out that (i) all the samples possess closed porosity, and (ii) the decrease in the surface area of laponite cannot be due to particles blocking more pores in this clay. Instead, a straightforward explanation is that the decrease is solely the result of the higher density of the iron oxide component (note that the density of the composites are of 23–26% higher than those of pure clays, as seen in table 1). For the better understanding of this issue, table 3 also includes SAXS surface areas related to the unit volume of the solid, besides that given in the conventional $m^2\ g^{-1}$ dimension. Surface areas specified to the volume reflect changes in the porous structure better as they are independent of the density differences. Indeed, the increment of the surface area upon iron oxide loading of montmorillonite is more pronounced, showing that this layer silicate suffers partial delamination in the composites and a more open structure is created. On the other hand, the great differences and clear trends in the surface areas of the laponite samples disappeared in this representation, which implies that the porous structure of the pure synthetic clay remains practically intact.

3.5. Mössbauer spectroscopy

Mössbauer spectroscopy is among the techniques that provide important information on the state of iron nuclei, and thus it is very useful for the characterization of the present composites, especially because XRD cannot discern between the isostructural magnetite and maghemite. In the following discussion, the interpretation of the spectroscopic data provide information on the iron oxide phases that the particles are composed of and on their superparamagnetic behaviour. The phenomenon of superparamagnetism in Mössbauer spectroscopy originates from the thermal fluctuations of fine particles that cause the direction of the associated magnetic moments to vary with a frequency (relaxation frequency) that depends upon the particle size, anisotropy energy, and temperature. If this frequency is greater than the Larmor frequency of the ^{57}Fe nucleus ($10^8\ s^{-1}$), the magnetic hyperfine splitting collapses and turns to a paramagnetic singlet or doublet. Around the transition temperature (blocking temperature) of the particles from the superparamagnetic to the magnetically ordered state, that is when their relaxation frequency approaches the Larmor frequency (10^7–$10^9\ s^{-1}$), the spectrum line can be a broad sextet with a distribution of hyperfine fields and a maximum field lower than that of the bulk material.

The Mössbauer experimental spectra recorded at room temperature (300 K) and liquid N_2 temperature (77 K) for Fe-Mont2 and Fe-Lap2 are shown in figures 5 and 6, along with the results of the mathematical deconvolution (upper spectra). The obtained hyperfine parameters are noted in table 4. Regarding Fe-Mont2, the room-temperature (RT) spectrum is composed of four sites. Site I corresponds to a sextet with a spectrum area of 63% and a hyperfine magnetic field value near the values of bulk maghemite or hematite. Site II (16%) with a distribution of hyperfine fields and a maximum value of 260 kOe originates from particles small enough that

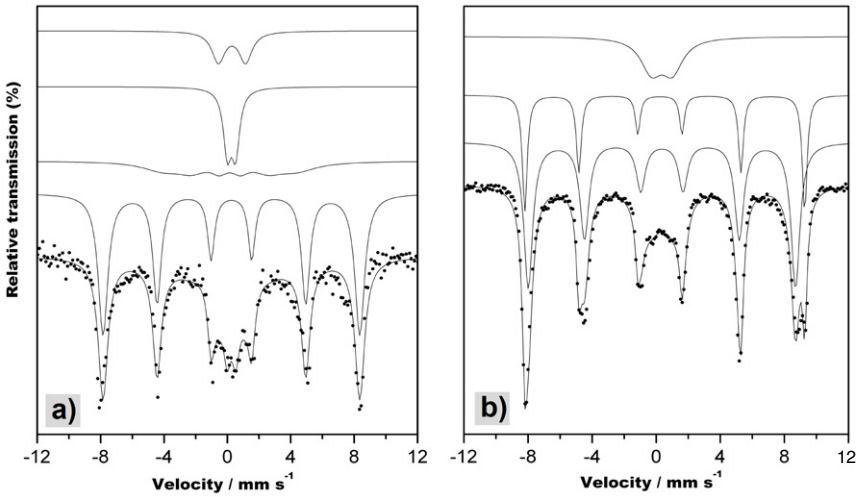

Figure 5. Mössbauer spectra of the sample Fe-Mont2 recorded at room temperature (a) and at liquid N_2 temperature (b). Dots represent the experimental data.

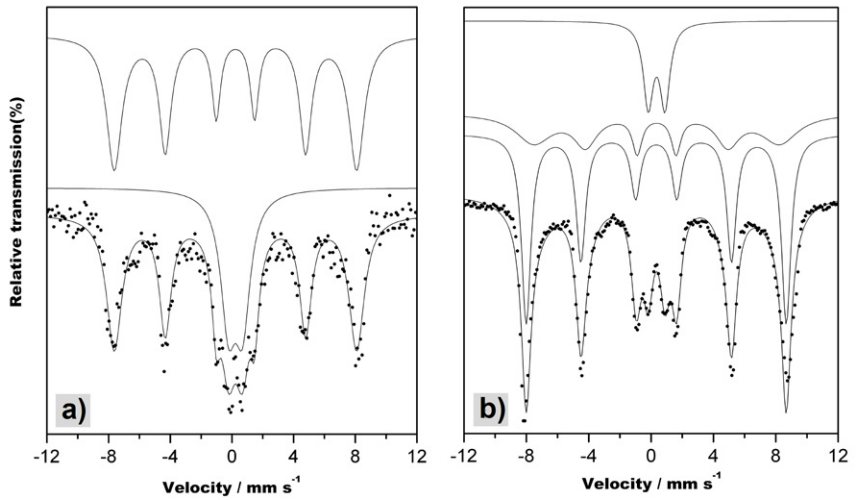

Figure 6. Mössbauer spectra of the sample Fe-Lap2 recorded at room temperature (a) and at liquid N_2 temperature (b). Dots represent the experimental data.

Table 4. Mössbauer spectra parameters of Fe-Mont2 and Fe-Lap2 composites. δ: isomer shift (mm s^{-1}, with respect to α-Fe), Γ: line width (mm s^{-1}), 2ε: quadrupole splitting (mm s^{-1}), H_{hf}: hyperfine field at iron nucleus (kOe), DH: distribution of hyperfine field and P: area percentage (%).

Sites	δ	Γ	$\Delta\varepsilon$	H_{hf}	DH	P	δ	Γ	$\Delta\varepsilon$	H_{hf}	DH	P
300 K			Fe-Mont2						Fe-Lap2			
I	0.36	0.50	0.00	505	8	63	0.33	0.56	0.00	490	20	68
II	0.36	0.60	0.52	0	0	12	0.34	1.20	0.92	0	0	32
III	0.26	0.77	0.00	260	74	16	—	—	—	—	—	—
IV	0.40	0.99	1.71	0	0	9	—	—	—	—	—	—
77 K			Fe-Mont2						Fe-Lap2			
I (mag)	0.46	0.67	0.00	520	0	59	0.44	0.74	0.00	520	0	56
II (hem)	0.46	1.60	0.66	0	0	15	0.46	0.77	1.07	0	0	13
III	0.49	0.36	0.30	544	0	26	0.46[a]	0.34	0.00	491	78	31

[a] Magnetite and hematite.

at this temperature they relax with frequencies approaching the Larmor frequency of the iron nucleus. Finally, sites III and IV are two quadrupole doublets (21% in total) arising from very small particles with relaxation frequency higher than the Larmor frequency of iron nucleus. Structural iron found in the octahedral positions of the montmorillonite sheet also

contributes to this doublet [29], the ratio of which to the total iron of the composite is ∼1.7 wt%, as estimated from ICP, unlike laponite, which does not contain any structural iron.

Turning to the liquid nitrogen (LN) spectrum, figure 5(b), we note that this consists of two well-resolved hyperfine sextets corresponding to 85% of the spectrum area and one paramagnetic broad doublet. The isomer shift values in all cases are typical of trivalent iron and the sextet I with hyperfine field of 520 kOe signals the formation of maghemite, (γ-Fe_2O_3) [30], while sextet II with a value of H_{hf} = 540 kOe indicates the formation of hematite, α-Fe_2O_3 [30]. The broad doublet (15%) involves the structural iron and very likely a fraction of particles with the smallest diameters, i.e. ∼5–10 nm, that have been detected by TEM measurements and are still superparamagnetic at 77 K. Note that the magnetically split lines become sharper and they gain intensity at the expense of the paramagnetic doublet, a feature that is characteristic of a superparamagnetic system consisting of magnetic particles with a distribution of sizes.

Concerning the laponite sample (Fe-Lap2), the spectrum at 77 K comprises a magnetic sextet (site I, 56%, H_{hf} = 520 kOe) corresponding to maghemite, a very broad sextet (site II, 31%) with low H_{hf} and a distribution of hyperfine fields attributed to very small particles whose thermal fluctuations are not yet totally suppressed at this temperature and finally one paramagnetic doublet (site III, 13%). Because of the relaxing state of the broad sextet, it cannot be solely ascribed to one of the two possible iron oxide phases (hematite or maghemite), but most likely its origin is attributed to small particles of both of the iron oxides. The doublet could be explained on the same basis as the doublet in the spectrum of Fe-Mont2, that is a superparamagnetic component ascribed to the fraction of the particles with the smallest diameters. The area percentage of the particles that appear to be in a relaxing state at 77 K is higher than the respective percentage for Fe-Mont2 sample, supporting the smaller particle formation on the laponite substrate.

In closing the Mössbauer analysis, a final comment should be made regarding the doublet lines at 77 K found in both samples, although it does not affect the general conclusions. Their origin could be attributed, at least partially, to paramagnetic iron atoms that are coordinated to the broken-bond sites (edges) of the external surfaces of the clays, which are the most reactive sites on a clay sheet [31]. These sites are small in number and are mainly found at the edges of the clay sheets due to the ending of the growing clay crystal. Nevertheless, during heat treatment the number of broken edges can be increased.

3.6. VSM measurements

To investigate the magnetic properties, the magnetization of the Fe-Mont2 and Fe-Lap2 composites versus the applied field was registered at ambient temperature. The magnetization curves (figure 7) showed no hysteresis and were completely reversible. Neither coercivity nor remanence magnetization was detected. Thus, it is apparent that the maghemite nanocrystals exhibit typical superparamagnetic behaviour, a property that is in close accordance with what was predicted from particle size and Mössbauer measurements.

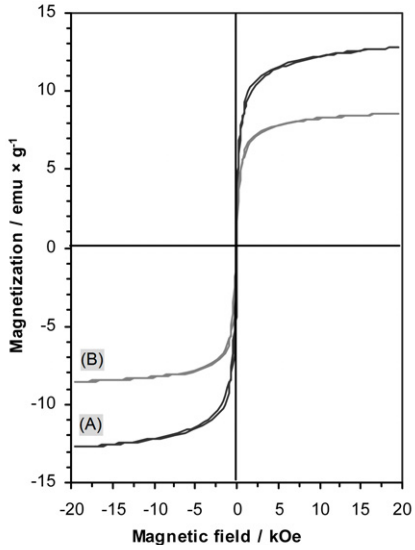

Figure 7. Magnetization versus magnetic field curves of (A) Fe-Lap2 and (B) Fe-Mont2 composites.

The saturation magnetization (M_S) of the composites was 8.56 emu g^{-1} for Fe-Mont2 and 12.8 emu g^{-1} for Fe-Lap2. Taking into account that the Fe_2O_3 content of both samples is nearly identical (32 wt%), it can be concluded that the laponite sample affords nanocomposites of higher magnetization. The saturation magnetization referring to the pure iron oxide phase in this latter composite is 40 emu g^{-1} and 27 emu g^{-1} for the Fe-Mont2 composite. Considering that Fe-Mont2 contains particles of higher diameters, the M_s values seem contradictory to this fact. Nevertheless, the lower maghemite content in the montmorillonite hybrid (as revealed by XRD) removes the contradiction. In addition, the presence of aggregated fine particles on the laponite substrate giving rise to superferromagnetism could be also related to the higher M_s value [32]. Finally, it should be noted that the higher extent of aggregation in the laponite composites, along with the size effect, is also related to the dominance of the maghemite phase due to the greater contribution of the attractive dipolar interactions between the magnetic nanocrystals.

4. Conclusions

In the present study, a natural and a synthetic layered silicate were primed with iron oxides by the same experimental procedure. Apart from their origin, the main differences between these clays are their lamellar sizes and their cation-exchange capacities. Our experiments clearly demonstrated that these factors influenced many of the observed properties of the clay composites. These characteristics are as follows: (1) average particle size, size distribution and aggregation state, (2) specific surface area, porous structure and the nanoscale dispersion of iron oxide crystals in the clay matrix, and (3) magnetic behaviour. As an ultimate conclusion, iron oxide/laponite composites enriched in ultrafine superparamagnetic γ-Fe_2O_3 particles are highly porous and possess significantly higher surface area and saturation magnetization as compared to the other clayey hybrid. Therefore, one great practical applicability of the

magnetically modified laponite lies in its improved capability to adsorb and separate a wide range of pollutants (due to its large surface area and magnetization) from aqueous or (due to the porosity) even from gaseous effluents.

Acknowledgments

This work was supported by a NATO collaborative linkage grant (PST CLG 980421) and a Greek–Hungarian Intergovernmental Science & Technology Cooperation. The authors thank Klára Kuhn for her technical assistance.

References

[1] Travis T 1993 *Chem. Ind—Lond.* **15** 581
[2] Cornell R M and Schwertmann U 1996 *The Iron Oxides. Structure, Properties, Reactions, Occurence and Uses* (Weinheim: VCH)
[3] Booker N A, Keir D, Priestley A, Rithchie C D, Sudarmana D L and Woods M A 1991 *Water Sci. Technol.* **123** 1703
[4] Oliveira L C A, Rios R V R A, Fabris J D, Sapag K, Garg V K and Lago R M 2003 *Appl. Clay Sci.* **22** 169
[5] Illés E and Tombácz E 2006 *J. Colloid Interface Sci.* **295** 115
[6] Tombácz E, Libor Z, Illés E, Majzik A and Klumpp E 2004 *Org. Geochem.* **35** 257
[7] Stavroyiannis S, Panagiotopoulos I, Niarchos D, Christodoulides J A, Zhang Y and Hadjipanayis G C 1998 *Appl. Phys. Lett.* **73** 3453
[8] Tsang S C, Yu C H and Tam K 2006 *J. Phys. Chem.* B **110** 16914
[9] Lee I S, Lee N, Park J, Kim B H, Yi Y-W, Kim T, Kim T K, Lee I H, Paik S R and Hyeon T 2006 *J. Am. Chem. Soc.* **128** 10658
[10] Mornet S, Vasseur S, Grasset F and Duguet E 2004 *J. Mater. Chem.* **14** 2161
[11] Sathe T R, Agrawal A and Nie S 2006 *Anal. Chem.* **78** 5627
[12] Wang D, He J, Rosenzweig N and Rosenzweig Z 2004 *Nano Lett.* **4** 409
[13] Skeff Neto K, Bakuzis A F, Pereira A R and Morais P C 2001 *J. Magn. Magn. Mater.* **226–230** 1893
[14] Galindo-González C, de Vincente J, Ramos-Tejada M M, López-López M T, González-Caballero F and Durán J D G 2005 *Langmuir* **21** 4410
[15] Muñoz B C, Adams G W, Ngo V T and Kitchin J R 2001 *US Patent Specification* 6,203,717 B1
[16] Kun R, Mogyorósi K and Dékány I 2006 *Appl. Clay Sci.* **32** 99
[17] Kőrösi L, Németh J and Dékány I 2004 *Appl. Clay Sci.* **27** 29
[18] Németh J, Dékány I, Süvegh K, Marek T, Klencsár Z, Vértes A and Fendler J H 2003 *Langmuir* **19** 3762
[19] Szabó T, Németh J and Dékány I 2003 *Colloids Surf.* A **230** 23
[20] Németh J, Rodriguez-Gattorno G, Olomos A V, Diaz D and Dékány I 2004 *Langmuir* **20** 2855
[21] Bourlinos A B, Devlin E, Boukos N, Simopoulos A and Petridis D 2002 *Clay Minerals* **37** 135
[22] Bourlinos A B, Karakassides M A, Simopoulos A and Petridis D 2000 *Chem. Mater.* **12** 2640
[23] Skoutelas A P, Karakassides M A and Petridis D 1999 *Chem. Mater.* **11** 2754
[24] van Duffel B and Schoonheydt R A 1999 *Langmuir* **15** 7520
[25] Morais P C, Gravina P P, Skeff Neto K and Lacava B M 2006 *Thin Solid Films* **515** 226
[26] Dékány I and Turi L 1997 *Colloids Surf.* A **126** 59
[27] Pernyeszi T and Dékány I 2003 *Colloid Polym. Sci.* **281** 73
[28] Dékány I and Turi L 1998 *Colloids Surf.* A **133** 233
[29] Reis A S Jr and Ardisson J D 2003 *Clays Clay Minerals* **51** 33
[30] Oh S J and Townsend H E 1998 *Hyperfine Interact.* **112** 59
[31] Pinnavaia T J and Beall G W 2000 *Polymer–Clay Nanocomposites* (*Wiley Series in Polymer Science*) (New York: Wiley)
[32] Bakuzis A F and Morais P C 2005 *J. Magn. Magn. Mater.* **285** 145